

Observation of Vortex Pinning in Bose-Einstein Condensates

S. Tung, V. Schweikhard, and E. A. Cornell
*JILA, National Institute of Standards and Technology, and Department of Physics,
 University of Colorado, Boulder, Colorado 80309-0440*
 (Dated: July 11, 2018)

We report the observation of vortex pinning in rotating gaseous Bose-Einstein condensates (BEC). Vortices are pinned to columnar pinning sites created by a co-rotating optical lattice superimposed on the rotating BEC. We study the effects of two types of optical lattice, triangular and square. In both geometries we see an orientation locking between the vortex and the optical lattices. At sufficient intensity the square optical lattice induces a structural cross-over in the vortex lattice.

PACS numbers: 03.75.Lm,74.25.Qt

Some of the most appealing results from recent work in superfluid gases have had to do with lattices, either optical lattices [1, 2, 3] or vortex lattices [4, 5, 6]. These two kinds of lattices could hardly be more different. The former is an externally imposed periodic potential arising from the interference of laser beams, while the latter is the self-organized natural response of a superfluid to rotation. As distinct as these two periodic structures may be, there are reasons for trying to marry them in the same experiment. For one thing, the extreme limits of rapid rotation (in the case of vortex lattices) [7] and deep potentials (in the case of optical lattices) [8] both lead to the same thing: correlated many-body states. For another, there is considerable precedent, from various subdisciplines of physics, for interesting effects arising from the interplay between competing lattices [9, 10, 11]. Moreover, the pinning of superconducting flux vortices to an array of pinning sites in solids is an area of very active research as well [12]. With these considerations in mind, we undertook a preliminary experimental study of the effects of a rotating optical lattice on a vortex lattice in a Bose-condensed sample of ^{87}Rb . The density of the superfluid is suppressed at the antinodes of the two-dimensional standing wave pattern of the optical lattice. These antinodes then become pinning sites, regions of low potential energy, for the superfluid vortices. Vortices can lower their interaction energy by arranging themselves to be as far apart as possible from one another. The competition between these effects has been examined in several theoretical works [13, 14]. Also [15, 16] discuss similar systems in the strong interacting regime

The setup for creating a rotating optical lattice is shown in Fig. 1(a). A mask with a set of holes is mounted onto a motor-driven rotary stage, and a laser beam (532 nm) is expanded, collimated, and passed through the mask. After the mask the resulting three beams are focused onto the Bose-Einstein condensates (BEC). The interference pattern at the focus constructs a quasi-2D optical lattice. The geometry and spatial extent of the triangular or the square optical lattice is determined by the size and layout of the holes and the focal length of the second lens. For the pinning sites to appear static

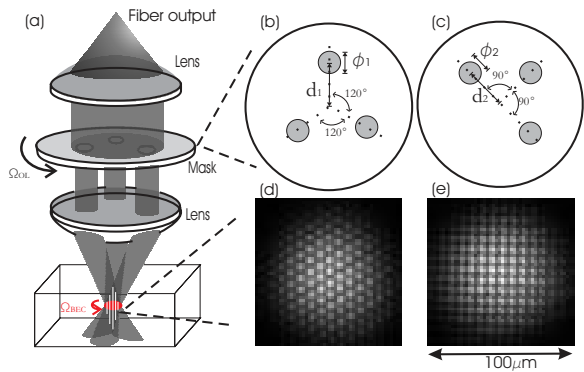


FIG. 1: (a) Schematic diagram of our setup for the rotating quasi-2D optical lattice. Layouts of the masks for a triangular (b) and square (c) optical lattices. (d) and (e) are pictures of triangular and square optical lattices, respectively. For details of the layouts see [17].

in the frame of a rotating BEC, the rotation of the two lattices must be concentric, and mechanical instabilities and optical aberrations (which lead to epicyclic motion of the pinning sites) must be particularly minimized. Even so, residual undesired motion is such that the strength of the optical lattice must be kept at less than 30% of the condensate's chemical potential or unacceptable heating results over the experiment duration of tens of seconds. We work in the weak pinning regime.

The experiments begin with condensates containing $\sim 3 \times 10^6$ ^{87}Rb atoms, held in the Zeeman state $|F = 1, m_f = -1\rangle$ by an axial symmetric magnetic trap with trapping frequencies $\{\omega_r, \omega_z\} = 2\pi\{8.5, 5.5\}\text{Hz}$. Before the optical lattice, rotating at angular frequency Ω_{OL} , is ramped on, the BEC is spun up [5] close to Ω_{OL} . This leads, before application of an optical lattice, to the formation of a near perfect triangular vortex lattice with a random initial angular orientation in inertial space. Through dissipation a vortex lattice can come to equilibrium with an optical lattice, with their rotation rates and angular orientations locked. In the absence of pinning sites, a vortex lattice with areal density of vortices n_v will rotate at (approximately [18, 19]) $\Omega = (\frac{\hbar\pi}{m})n_v$.

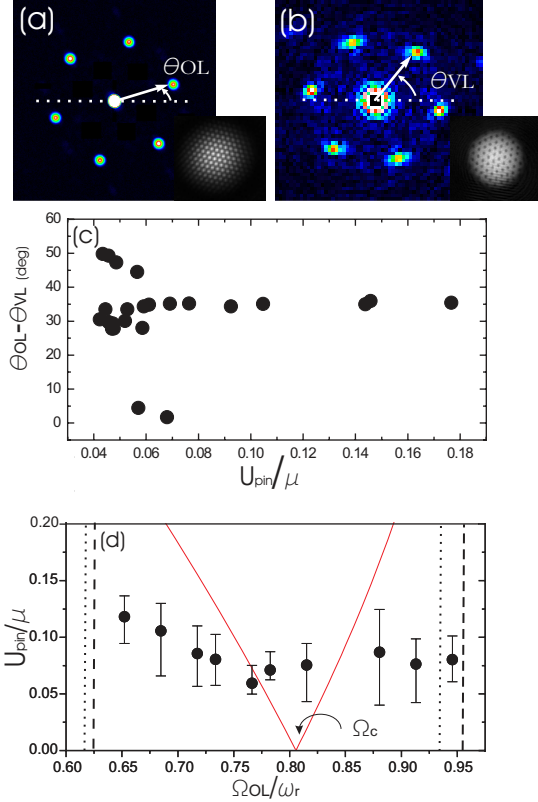


FIG. 2: (a) Triangular optical lattice and (b) vortex lattice in reciprocal space. Each inset shows the corresponding original real-space CCD-camera images. (c) The difference in orientation $\theta_{OL} - \theta_{VL}$ versus the strength of pinning U_{pin}/μ (the peak of the optical potential normalized by the condensate's chemical potential) for the rotation rates $\Omega_{OL} = 1.133\Omega_c = 0.913\omega_r$. With increasing pinning strength, $\theta_{OL} - \theta_{VL}$ tends towards its locked value [20]. (d) Minimum pinning strength needed for orientation locking between two lattices as a function of the rotation rate of the optical lattice. The dashed and dotted lines are discussed in the text.

This suggests that for an optical lattice with an areal density of pinning sites n_{OL} , locking between the two lattices will be facilitated if the optical lattice rotates at the commensurate frequency $\Omega_c \equiv (\frac{\hbar\pi}{m})n_{OL}$.

We measure the angular difference $\theta_{OL} - \theta_{VL}$ between the orientation of the optical and vortex lattice in reciprocal space (see Figs. 2(a)–2(b)). Fig. 2(c) shows $\theta_{OL} - \theta_{VL}$ as a function of the pinning strength with an optical lattice rotation rate $\Omega_{OL} = 1.133\Omega_c = 0.913\omega_r$. The strength of pinning is characterized by the ratio U_{pin}/μ (μ is the chemical potential of the condensate [21]), which gives the relative suppression of the superfluid density at pinning sites. We can see the initially random angular difference between the two lattices becomes smaller as the pinning strength U_{pin}/μ increases. For $U_{pin}/\mu \gtrsim 0.08$, the angular differences become very close to the locked value. Figure 2(d) shows the phase diagram. The data points and error bars mark the mini-

mum pinning strength $(U_{pin}/\mu)_{min}$ above which the lattices lock. We observe two distinct regimes. First, for small rotation-rate mismatch, $(U_{pin}/\mu)_{min}$ is rather independent of the rotation-rate mismatch. Second, for rotation-rate mismatch beyond the range indicated by the dashed line in Fig. 2(d), angular orientation locking becomes very difficult for any U_{pin}/μ in our experiment. Instead, an ordered vortex lattice with random overall angular orientation observed at low U_{pin}/μ transforms into a disordered vortex arrangement at high U_{pin}/μ .

This box-like shape of the locked region in $U_{pin} - \Omega_{OL}$ space is worth considering. In a simple model, vortex motion in our system is governed by a balance of the pinning force and the Magnus force. The pinning force is $\vec{F}_{pin}(x) \propto U_{pin}/d$, where U_{pin} and d are the strength of the pinning potential and its period, respectively. The Magnus force, acting on a vortex moving with velocity \vec{v}_{vortex} in a superfluid with velocity \vec{v}_{fluid} is $\vec{F}_{mag}(x) \propto n(x)(\vec{v}_{vortex} - \vec{v}_{fluid}) \times \vec{\kappa}$ where $\vec{\kappa} = (\frac{\hbar}{m})\hat{z}$, and $n(x)$ is the superfluid density. A locked vortex lattice will co-rotate with the pinning potential, giving $\vec{v}_{vortex}(r) = \vec{v}_{OL}(r) = \vec{\Omega}_{OL} \times \vec{r}$, whereas the superfluid velocity in a solid-body approximation is $\vec{v}_{fluid}(r) = \frac{\hbar\pi}{m}n_v r\hat{\theta} = \vec{\Omega}_{fluid} \times \vec{r}$. Comparing the magnitudes of both forces at $r = R(\Omega)/2$, where $R(\Omega)$ is the centrifugal-force modified Thomas-Fermi radius, we obtain a minimum strength for pinning $(U_{pin}/\mu)_{min} \approx (\frac{1}{2\sqrt{3}}R(\Omega)/d) \times (\Omega_{OL} - \Omega_{fluid})/\Omega_c$.

What will be the fluid rotation rate Ω_{fluid} in the presence of the pinning potential? On the one hand, if vortices are tightly locked to the optical lattice sites, we have $\Omega_{fluid} = \Omega_c$. The minimum strength $(U_{pin}/\mu)_{min}$ resulting from this assumption is plotted as solid line in Fig. 2(d). The lack of predicted decrease of $(U_{pin}/\mu)_{min}$ to zero around Ω_c may be due to long equilibration times in a very shallow pinning potential, as well as slight mismatches in alignment and initial rotation rate of the BEC and the pinning potential. The ease of orientation locking with increasing rotation rate mismatch is less easy to explain in this model. On the other hand, in the weak-pinning regime, the vortex lattice can accommodate a rotation rate mismatch by stretching/compressing away from the pinning sites. This allows the fluid to co-rotate with the optical lattice ($\Omega_{fluid} \approx \Omega_{OL}$) and reduce the Magnus force. This leads to a very low minimum pinning strength, as suggested by our data. However, the vortex lattice's gain in pinning energy decreases rapidly in the locked orientation when the mismatch between vortex spacing and optical lattice constant increases to the point where the outermost vortices fall radially in between two pinning sites. Then the preference for the locked angular orientation vanishes. This predicted limit is indicated by the vertical dotted lines in Fig. 2(d).

In the absence of a pinning potential, the interaction energy of a square vortex lattice is calculated to exceed

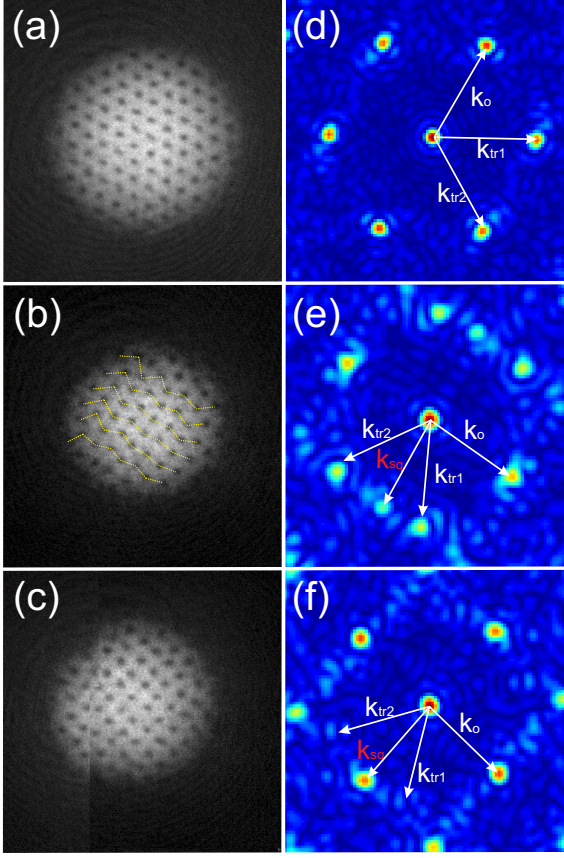


FIG. 3: Images of rotating condensates pinned to an optical lattice at $\Omega_{OL} = \Omega_c = 0.866\omega_r$ with pinning strength $U_{pin}/\mu =$ (a) 0.049 (b) 0.084 (c) 0.143, showing the structural cross-over of the vortex lattice. (a)–(c) are the absorption images of the vortex lattices after expansion. (d)–(f) are the Fourier transforms of the images in (a)–(c). k_o is taken by convention to be the strongest peak; k_{tr1} , k_{sq} , and k_{tr2} are at 60° , 90° , and 120° , respectively, from k_o .

that of a triangular lattice by less than 1% [22], thus it is predicted [13, 14] that the influence of even a relatively weak square optical lattice will be sufficient to induce a structural transition in the vortex lattice. This structural cross-over of a vortex lattice is observed in our experiment. Figure 3 shows how the vortex lattice evolves from triangular to square as the pinning strength increases. Over a wide range of pinning strengths, we observe that there is always at least one lattice peak in reciprocal space that remains very strong. We define this peak to be k_o . Lattice peaks at 60° and 120° from k_o are referred to as k_{tr} , and, together with k_o , their strength is a measure of the continued presence of a triangular lattice. A peak at 90° , referred to as k_{sq} , is instead a signal for the squareness of the vortex lattice. With increasing pinning strength (Fig. 3(a–c), or (d–f)), we see the triangle to square crossover evolve. At intermediate strengths ($U_{pin}/\mu = 0.084$), a family of zigzag vortex rows emerges, indicated by the dotted lines in Fig. 3(b); in reciprocal

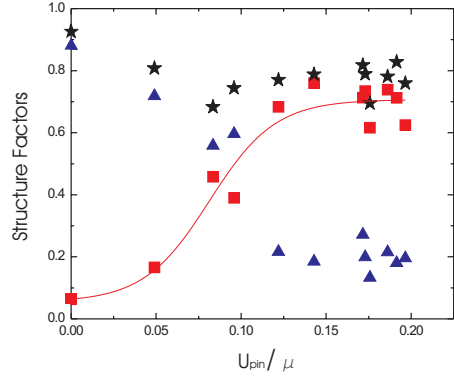


FIG. 4: Structure factors (a) $|S(k_{sq})|$ (■), (b) $|S(k_{tr})|$ (▲) (average of $|S(k_{tr1})|$ and $|S(k_{tr2})|$), and (c) $|S(k_o)|$ (★) versus the strength of the pinning lattice at the commensurate rotation rate Ω_c . $|S(k_{sq})|$ is fitted by [23]. The fitting leads to a maximum value 0.707 of $|S(k_{sq})|$. An ideal square vortex lattice would have $|S(k_{sq})|=1$.

space we see the presence of structure at k_{tr} and k_{sq} .

We quantify the crossover by means of an image-processing routine that locates each vortex core, replaces it with a point with unit strength, Fourier transforms the resultant pattern, and calculates structure factors $|S|$ [14] based on the strength of the images at lattice vectors k_{sq} , k_{tr} , and k_o . In Fig. 4, we see with increasing optical potential the turn-on of $|S(k_{sq})|$ balanced by the turn-off of $|S(k_{tr})|$. We use a fitting function to smooth the noisy data of $|S(k_{sq})|$. The structure crossover takes place around $U_{pin}/\mu \approx 8\%$, in rough agreement with predictions of $U_{pin}/\mu \approx 5\%$ from numerical simulations [14] and $U_{pin}/\mu \approx 1\%$ from analytic theory for infinite lattices [13]. The fact that one lattice peak remains strong for all pinning strengths (the stars (★) in Fig. 4) suggests that as the pinning strength is increased, one family of vortex rows represented by k_o in Fourier space locks to the square pinning lattice and remains locked as the shape cross-over distorts the other two families of vortex rows into a square geometry. The effects of various rotation rates and optical potential strengths on the squareness of the vortex lattice is summarized in Fig. 5. We surmise that there are a number of effects at play. When Ω_{OL} differs from Ω_c , pinning strength is required not only to deform the shape of the vortex lattice from triangular to square, but also to compress or expand it to match the density of the optical lattice sites. At higher optical intensities, we know from separate observations that imperfections in the rotation of the optical lattice lead to heating of the condensate, which may limit the obtainable strength of the square lattice.

A dumbbell-shape lattice defect (Fig. 6) is sometimes observed in the early stages of the square vortex lattice formation when $\Omega_{OL} > \Omega_c$. In the weak-pinning regime,

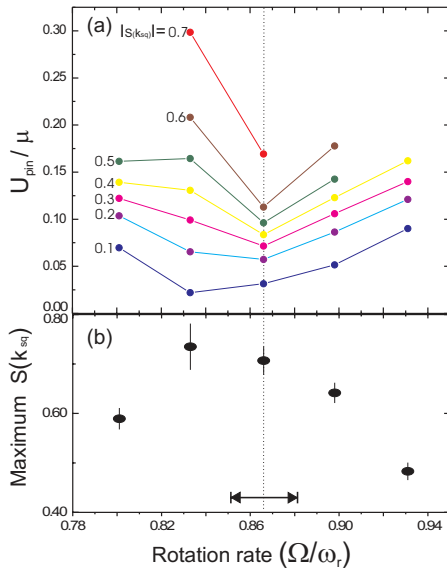


FIG. 5: Effect of square pinning lattice. (a) Contours of $|S(k_{sq})|$ are plotted, showing the effect of the rotation rate and pinning strength on the squareness of the vortex lattice. (b) The maximum observed squareness. In (a) and (b), for each rotation rate, the data points are extracted from fits such as that shown in Fig. 4 for $\Omega_{OL} = \Omega_c$. The vertical dotted line plus arrow shows the possible range of Ω_c consistent with the uncertainty in n_{OL} .

the defect will relax towards the equilibrium configuration by pushing extra vortices at the edge of the condensate outside the system. Defects of this nature, involving extra (or missing) vortices, are the exception and not the rule in our observations, even for $\Omega_{OL} \neq \Omega_c$. In an infinite system, the physics of the lattice-lattice interaction would likely be dominated by these point defects. In our finite system, would-be incommensurate lattices can accommodate by stretching or compressing.

The work presented in this paper was funded by NSF and NIST. We would like to acknowledge P. Engels and M. Friedman for help with the early experimental setup. We would also like to thank A. Leanhardt, D. Sheehy, M. Kraemer, and R. Bhat for useful discussion and H. Green for helping manufacture the rotating masks.

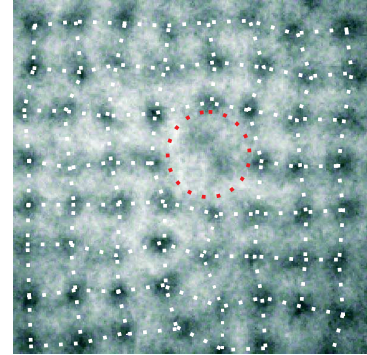


FIG. 6: Image of a dumbbell-shape defect consisting of two vortices locked to one pinning site during the formation of the square vortex lattice. Dotted lines are to guide the eye.

(2004).

- [6] J. R. Abo-Shaeer, C. Raman, J. M. Vogels, and W. Ketterle, *Science* **292**, 476 (2001).
- [7] N. R. Cooper, N. K. Wilkin, J. M. F. Gunn, *Phys. Rev. Lett.* **87**, 120405 (2001).
- [8] D. Jaksch, C. Bruder, J. I. Cirac, C. W. Gardiner, and P. Zoller, *Phys. Rev. Lett.* **81**, 3108 (1998).
- [9] P. W. Stephens *et al.*, *Phys. Rev. B* **29**, 3512 (1984).
- [10] P. Bak, *Rep. Prog. Phys.* **45**, 587 (1982).
- [11] T. Goto, T. Kimura, G. Lawes, A. P. Ramirez, and Y. Tokura, *Phys. Rev. Lett.* **92**, 257201 (2004).
- [12] M. Baert *et al.*, *Phys. Rev. Lett.* **74**, 3269 (1995); A. N. Grigorenko *et al.*, *Phys. Rev. Lett.* **90**, 237001 (2003); J. E. Villegas *et al.*, *Science* **302**, 1188 (2003); C. Reichhardt *et al.*, *Phys. Rev. B* **64**, 144509 (2001).
- [13] J. W. Reijnders and R. A. Duine, *Phys. Rev. Lett.* **93**, 060401 (2004); J. W. Reijnders and R. A. Duine, *Phys. Rev. A* **71**, 063607 (2005).
- [14] H. Pu, L. O. Baksmaty, S. Yi, and N. P. Bigelow, *Phys. Rev. Lett.* **94**, 190401 (2005).
- [15] Congjun Wu, Han-dong Chen, Jiang-piang Hu, and Shou-Cheng Zhang, *Phys. Rev. A* **69**, 043609 (2004).
- [16] Rajiv Bhat, L. D. Carr, and M. J. Holland, *Phys. Rev. Lett.* **96**, 060405 (2006).
- [17] Mask (b): $\phi_1 = 2.5$ mm and $d_1 = 11.5$ mm. The lattice constant of the triangular optical lattice is $7.8 \mu\text{m}$, giving $\Omega_c = 0.806 \omega_r$; Mask (c): $\phi_2 = 2.5$ mm and $d_2 = 13.5$ mm. The lattice constant of the square lattice is $7.0 \mu\text{m}$, giving $\Omega_c = 0.866 \omega_r$. The focal lens of two lenses are 300 mm and 250 mm, respectively.
- [18] I. Coddington *et al.*, *Phys. Rev. A* **70**, 063607 (2004).
- [19] Daniel E. Sheehy and Leo Radzihovsky, *Phys. Rev. A* **70**, 051602(R) (2004).
- [20] There is a constant measurement offset to the values of $\theta_{OL} - \theta_{VL}$ in this data set. We have used in-trap images of vortex lattices to confirm that the absolute value of $\theta_{OL} - \theta_{VL}$ is zero for locked lattices
- [21] The chemical potential is determined from the axial Thomas-Fermi radius of the condensate obtained from in-trap images, and is proportional to the peak density of the condensate.
- [22] L. J. Campbell, M. M. Doria, J. B. Kaduk, *Phys. Rev.*

A **39**, 5436 (1989).
[23] $|S(k_{sq})| = A_2 + \{(A_1 - A_2)/(1 + \text{Exp}[(U - U_0)/(\delta U)])\};$

A_1 , A_2 , U_0 , and δU are fit to the data.